energies

MDPI

Article

A Comparative Study of Fission Yield Libraries Between ORIGEN2 and ENDF/B-VIII.0 for Molten Salt Reactor Burnup Calculation

Yunfei Zhang, Guifeng Zhu, Yang Zou *, Jian Guo, Bo Zhou, Rui Yan and Ao Zhang

National Key Laboratory of Thorium Energy, Shanghai Institute of Applied Physics, Chinese Academy of Sciences, Shanghai 201800, China; zhangyunfei@sinap.ac.cn (Y.Z.)
* Correspondence: zouyang@sinap.ac.cn

Abstract

As a promising nuclear technology, molten salt reactors (MSRs) have a bright future in the energy sector due to their unique advantages such as high efficiency, safety, and fuel flexibility. However, the accurate analysis of fission products in MSRs requires reliable fission yield data. Current reactor burnup analysis often uses the ORIGEN2 code, whose fission yield libraries mainly originate from the outdated 1970s ENDF/B-VI nuclear database, thus risking data obsolescence. This study evaluates ORIGEN2's fission yield libraries (THERMAL, PWRU, PWRU50) against the modern ENDF/B-VIII.0 library. Through a comprehensive comparative analysis of Oak Ridge National Laboratory's Molten Salt Reactor Experiment (MSRE) model, numerical simulations reveal library-dependent differences in MSR burnup characteristics. The PWRU library best matches ENDF/B-VIII.0 for U-235-fueled cases in keff results, while the PWRU50 library has minimal keff deviation in U-233-fueled setups. Moreover, in both fuel cases, the fission yield library was found to significantly affect the activity of key radionuclides, including Kr-85, Kr-85m, I-133m, Cs-136, Sn-123, Sn-125, Sn-127, Sb-124, Sb-125, Cd-115m, Te-125m, Te-129m, etc. Additionally, the fission gas decay heat power calculated via the ORIGEN2 library is over 20% lower than that from the ENDF/B-VIII.0 library tens of days after shutdown, mainly due to differences in long-lived Kr-85 production. These findings highlight the need to update traditional fission yield libraries in burnup codes. For next-generation MSR designs, this is crucial to ensure accurate safety assessments and the effective development of this promising energy technology.

Keywords: fission yield; ORIGEN2; ENDF/B-VIII.0; MSRE

check for updates

Academic Editor: Sung Joong Kim

Received: 13 May 2025
Revised: 1 July 2025
Accepted: 4 July 2025
Published: 6 July 2025

Citation: Zhang, Y.; Zhu, G.; Zou, Y.; Guo, J.; Zhou, B.; Yan, R.; Zhang, A. A Comparative Study of Fission Yield Libraries Between ORIGEN2 and ENDF/B-VIII.0 for Molten Salt Reactor Burnup Calculation. *Energies* **2025**, *18*, 3562. https://doi.org/10.3390/en18133562

Copyright: © 2025 by the authors. Licensee MDPI, Basel, Switzerland. This article is an open access article distributed under the terms and conditions of the Creative Commons Attribution (CC BY) license (https://creativecommons.org/licenses/by/4.0/).

1. Introduction

The nuclear energy landscape is undergoing a transformative shift toward advanced reactor systems that promise enhanced safety, sustainability, and fuel cycle flexibility. The Molten Salt Reactor Experiment [1–3] (MSRE), the first liquid-fuel reactor developed by the US Oak Ridge National Laboratory in the 1960s, has recently garnered renewed attention in Generation IV nuclear systems and advanced fuel cycle research due to its unique molten salt fuel cycle and Th-U breeding potential. Initially using U-235 and later switching to U-233 dissolved in LiF-BeF_2-ZrF_4 fuel salt [4], the MSRE demonstrated liquid-fuel reactor feasibility and provided valuable data on fission product behavior, corrosion dynamics, and neutron economy. During operation, fission products formed in the molten fuel salt

were distributed across the primary loop. Their distribution and behavior were influenced by volatility, fuel salt solubility, and chemical interactions with structural materials. Volatile fission gases like Kr and Xe isotopes were continuously removed via a helium bubbling system [5], while refractory metal nuclides accumulated locally. Some fission products also underwent chemical reactions with the fuel salt or reactor materials, forming different chemical species. Accurately modeling fission product source terms in molten salt reactors is crucial, as inaccurate fission yield data can lead to a misestimation of key radionuclide activities, affecting assessments of decay heat, radiation levels, and environmental impacts.

ORIGEN2 [6–8] is a typical single-group point-depletion and decay irradiation calculation code developed by Oak Ridge National Laboratory in the United States. Due to its simple usage, high computational efficiency, and flexible external databases, it is still widely used for calculations and research in the fields of reactor activation and source term analysis. The fission yield data used in ORIGEN2 is mainly taken from the nuclear evaluation database ENDF/B-IV [9], which has been around for more than 40 years. With the rapid development of advanced reactors and the continuous improvement of design and computing requirements, nuclear databases are also constantly iterating. At present, many studies on the burnup and source term of molten salt reactors are still based on the fission yield database of ORIGEN2. Using outdated fission yield data may result in insufficient calculation accuracy. Therefore, this study compares the thermal reactor-specific fission yield databases (THERMAL, PWRU, and PWRU50) [6] in ORIGEN2 with the ENDF/B-VIII.0 [10]-based yields using the MSRE model. The evaluation focuses on depletion neutronics, fission product source terms, and decay heat. By quantifying the differences between these databases, this study offers a quantitative reference for database selection in molten salt reactor burnup and source term calculations, thus enhancing reactor safety analysis accuracy.

The structure of this paper is outlined as follows: Section 2 delineates the databases and simulation code. Section 3 analyzes the difference of fission yield between ORIGEN2 and ENDF/B-VIII.0. Finally, Section 4 presents the conclusions drawn from this study.

2. Databases and Calculation Tool

2.1. Neutron-Induced Fission Yield Data in ORIGEN2

The ORIGEN2 package boasts an extensive collection of over fifty different cross-section and fission yield libraries, spanning various reactor system types that users can select based on their specific requirements. The prefabricated one-group cross-sections and fission yields of fission products are stored in the same file. Among these libraries, approximately ten libraries are tailored for pressurized water reactors (PWRs). There are also libraries applicable to boiling water reactors (BWRs), heavy water reactors (HWRs), and liquid metal fast reactors (LMFRs). Each library specifies the fission yields of eight actinides (Th-232, U-233, U-235, U-238, Pu-239, Pu-241, Cm-245, and Cf-252), and contains more than 800 fission products. All the fission yield data of the fission products are independent yields, mostly taken from ENDF/B-IV.

In this study, three thermal spectrum reactor-related fission yield libraries from ORIGEN2 were selected for analysis, namely THERMAL, PWRU, and PWRU50. Notably, the THERMAL library is designed for thermal spectrum reactor calculations, the PWRU library is specifically designed for typical PWRs fueled by U-235-enriched UO_2 and operated at a burnup depth of 33,000 MWd/MTU and for PWRU50 a depth of 50,000 MWd/MTU.

2.2. Neutron-Induced Fission Yield Data in ENDF/B-VIII.0

The neutron-induced independent fission yield data in ENDF/B-VIII.0 cover 31 actinides. A total of 12 of these actinides have fission yield data for up to three en-

ergy points (0.0253 eV, 0.5 MeV, and 14 MeV, as shown in Table 1). Pu-239 also offers fission yield data for the 2 MeV energy point. Each actinide fission yields more than 1000 fission product nuclides. The fission yield database in ENDF/B-VIII.0 is largely derived from ENDF/B-VI.8, and the independent neutron-induced fission yields are represented by MT/MF = 8/454 in the ENDF-6 format. When calculating the depletion problem of the Molten Salt Reactor Experiment (MSRE), the fission yield data at the nearest energy point in ENDF/B-VIII.0 are used, which are the energy points highlighted in bold red in Table 1.

Table 1. Fission yield settings in ENDF/B-VIII.0.

Actinides	0.0253 eV	0.5 MeV	14 MeV
Th-227	√		
Th-229	√		
Th-232		√	√
Pa-231		√	
U-232	√	√	√
U-233	√	√	√
U-234		√	√
U-235	√	√	√
U-236		√	√
U-237		√	
U-238		√	√
Np-237	√	√	√
Np-238		√	
Pu-238		√	
Pu-239	√	√	√
Pu-240	√	√	√
Pu-241	√	√	
Pu-242	√	√	√
Am-241	√	√	√
Am-242m	√		
Am-243		√	
Cm-242		√	
Cm-243	√	√	
Cm-244		√	
Cm-245	√		
Cm-246		√	
Cm-248		√	
Cf-249	√		
Cf-251	√		
Es-254	√		
Fm-255	√		

Figures 1 and 2, respectively, present the comparison of fission product yields for U-235 and U-233 between the ENDF/B-VIII.0 library and the ORIGEN2 library. From the figures, it can be clearly observed that compared with the earlier ORIGEN2 library, the modern ENDF/B-VIII.0 library provides more comprehensive and detailed fission yield data. Furthermore, numerous fission product yields in the ORIGEN2 library exhibit significant deviations from the corresponding data in the ENDF/B-VIII.0 library. It should be noted that the fission yield libraries in ORIGEN2 provide fission yields for light nuclei such as H-3, Li-6, Li-7, Be-9, Be-10, and C-14, which are not included in ENDF/B-VIII.0. While tritium (H-3) is significant in a source term analysis, its primary production pathway in molten salt reactors (MSRs) containing Li-6 arises from the (n, T) reaction of Li-6. Therefore, this discrepancy has minimal impact on MSR applications. In summary, there exists substantial discrepancy between the fission yield data in ORIGEN2 and those in the

advanced ENDF/B-VIII.0 library. This significant inter-database discrepancy will directly affect the computational accuracy of cumulative fission product inventories, particularly in long-term burnup calculations, where error propagation effects may lead to excessive evaluation deviations in critical safety parameters (such as decay heat and radiation source terms), thereby impacting the reactor design and safety analysis.

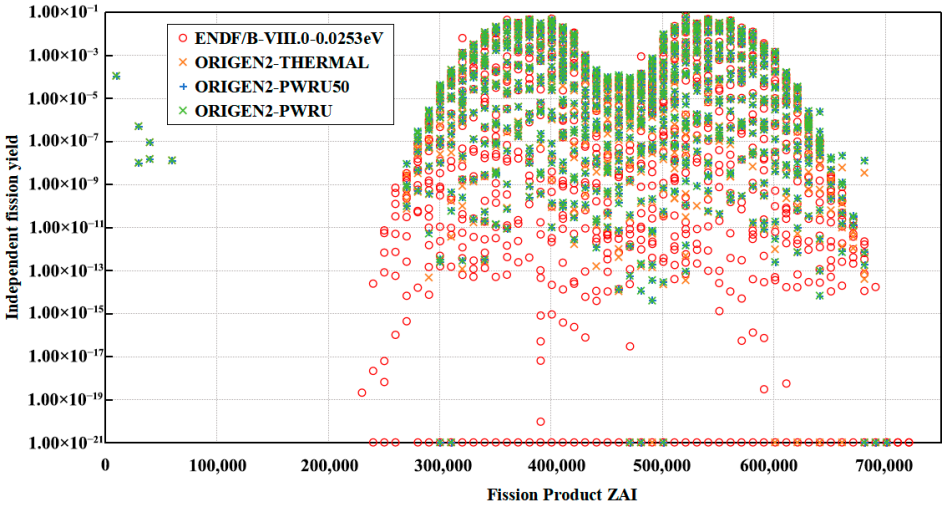


Figure 1. Comparison of fission yields for U-235.

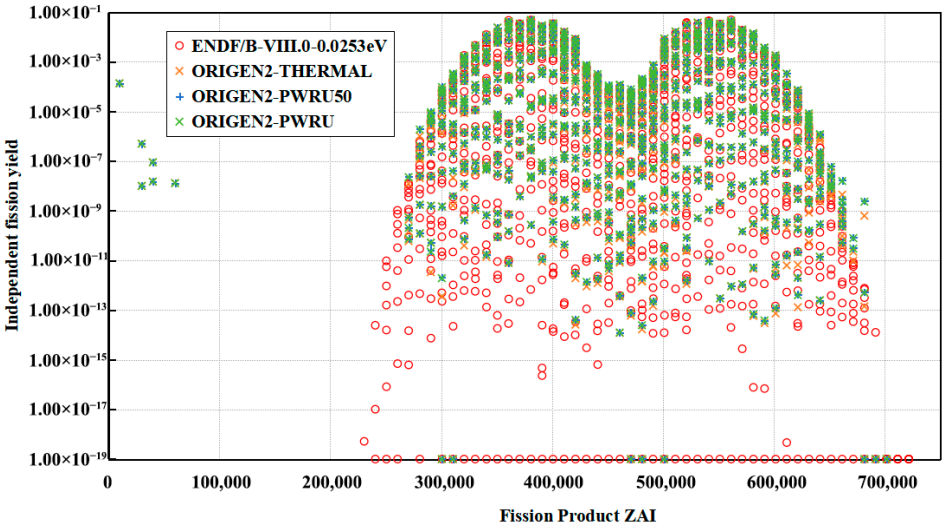


Figure 2. Comparison of fission yields for U-233.

2.3. MSR Depletion Code MACT

MACT [11] is a home-developed depletion and source term calculation program for molten salt reactors (MSRs) based on the C language. In addition to the traditional depletion calculation functions for solid-fuel reactors, it also supports continuous fueling, reprocessing, and flow depletion issues for liquid molten salt reactors. MACT employs the widely used "ZAI" nuclide naming convention, where the nuclide ID is calculated as 10,000 × Z + 10 × A + IS. Here, Z represents the atomic number (number of protons), A is the mass number, and IS indicates whether the nuclide is in an excited state (1 for an excited state, 0 for a ground state). The current version of MACT uses a depletion library containing approximately 1500 nuclides, sourced from ORIGEN2 and ORIGEN-S. Neutron reactions include (n,γ), (n,f), (n,2n), (n,3n), (n,α), and (n,p) reactions, with a prefabricated set of microscopic cross-sections and thermal-spectrum fission product yields.

Decay reactions encompass α decay, β decay, β + n decay, electron capture, and isomeric transition decay from excited states to a ground state. In solving the depletion equations, the solution algorithm employs the widely adopted Chebyshev Rational Approximation Method [12,13] (CRAM) and the transmutation trajectory analysis [14] (TTA). MACT supports three calculation modes: constant power calculation, constant flux calculation, and decay calculation. In terms of physical quantity output, it supports the output of parameters such as nuclide density, radioactive activity, decay heat power, and photon emission intensity. MACT has been coupled with the open-source Monte Carlo software OpenMC(version 0.15.0) [15] using the predictor–corrector method, enabling MSR depletion calculations with updated reaction rates.

3. Numerical Results

The reactor core model employed in this research is the Molten Salt Reactor Experiment (MSRE) developed by the Oak Ridge National Laboratory in the United States. The MSRE adopted LiF-BeF2-ZrF4-UF4 (in a molar ratio of 65:29:5:1) as the fuel salt, featuring a U-235 enrichment of 33%. Graphite served as the moderator material, while the structural material was a nickel-based Hastelloy N alloy. The detailed compositions of the fuel salt, graphite, and structural material are shown in Table 2. The numerical simulation was set to operate the reactor continuously for 10 years under the conditions of a thermal power of 8 MW and a core operating temperature maintained at 900 K. The depletion code MACT, coupled with OpenMC, was used to perform constant-power depletion calculations, with a focus on examining the impact of different fission yield databases on the calculation results under U-235 and U-233 loadings. A simplified MSRE model was established with uniform infinite extension along the axial (Z-axis) direction and the cross-sectional view of the MSRE core modeled in OpenMC is shown in Figure 3. Each case executed 80 generations of particle histories, with the first 30 generations skipped as inactive cycles, and the number of particles tracked per generation set at 50,000. Under this particle setting, the statistical deviation of the effective multiplication factor obtained from each transport calculation was within the range of 50 to 70 pcm. In all numerical cases, 140 key nuclides were explicitly modeled in OpenMC at each burnup calculation step, while cross-sections for the remaining nuclides were uniformly invoked from the pre-stored data in the MACT database.

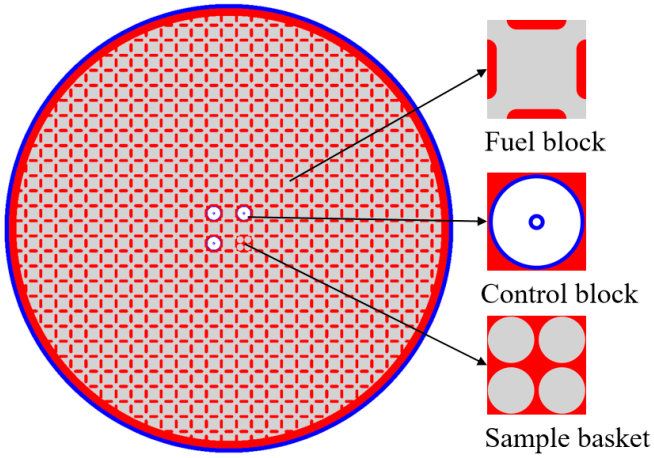


Figure 3. Cross-sectional view of the MSRE core modeled with OpenMC.

Table 2. Composition of fuel salt, graphite, and structural material.

	Nuclide	Atom number density ($barn^{-1}cm^{-1}$)		Nuclide	Weight percent
Fuel salt	Li-6	1.0976×10^{-6}	Structural material (8.7745 g/cm^3)	Ni	0.685
	Li-7	2.1951×10^{-2}		Co	0.002
	Be-9	9.8617×10^{-3}		Cr	0.007
	F-19	4.9511×10^{-2}		Mo	0.165
	Zr-90	8.6881×10^{-4}		Fe	0.05
	Zr-91	1.8947×10^{-4}		Si	0.01
	Zr-92	2.8960×10^{-4}		Cu	0.0035
	Zr-94	3.4077×10^{-4}		Mn	0.01
	U-234	8.5264×10^{-7}		C	0.0006
	U-235	8.5446×10^{-5}		Ti	0.0025
	U-236	3.6231×10^{-7}		Al	0.0025
	U-238	1.8352×10^{-4}		S	0.0002
Graphite	Nuclide	Atom number density ($barn^{-1}cm^{-1}$)		B	0.0001
	C-12	9.2237×10^{-2}		W	0.005
	C-13	1.0259×10^{-3}		P	0.00015

3.1. Effective Multiplication Factor

When operating with U-235, Figure 4 compares the effective multiplication factors (keff) calculated using the three fission yield databases in ORIGEN2 with those obtained using ENDF/B-VIII.0 for the MSRE. Over 10 years of full-power operation, the maximum deviations from ENDF/B-VIII.0 were 329.0 pcm for the THERMAL library, 250.2 pcm for the PWRU50 library, and 243.8 pcm for the PWRU library. The figure also shows keff calculations considering the removal of fission gases (all Kr and Xe isotopes) at a rate of 2.05419×10^{-4} s^{-1} [16]. In these cases, the deviations were 270.4 pcm (THERMAL), 290.0 pcm (PWRU50), and 240.8 pcm (PWRU). Overall, for the U-235-fueled MSRE, the calculated effective neutron multiplication factors from the PWRU fission yield library demonstrate the closest agreement with those from the ENDF/B-VIII.0 library.

For the U-233-fueled operation (with only the fuel salt's initial U-235 replaced by U-233, and the other conditions unchanged), Figure 5 shows the database comparisons. Over 10 years of full-power operation, the deviations from the ENDF/B-VIII.0-based keff were 292.0 pcm (THERMAL), 178.0 pcm (PWRU50), and 218.0 pcm (PWRU). When considering Kr and Xe isotope removal, the deviations were 247.0 pcm (THERMAL), 242.0 pcm (PWRU50), and 265.0 pcm (PWRU). In summary, under the U-233-fueled operational conditions of the Molten Salt Reactor Experiment (MSRE), the keff values derived from the PWRU50 fission yield library demonstrated closer agreement with the reference results from the ENDF/B-VIII.0 benchmark library.

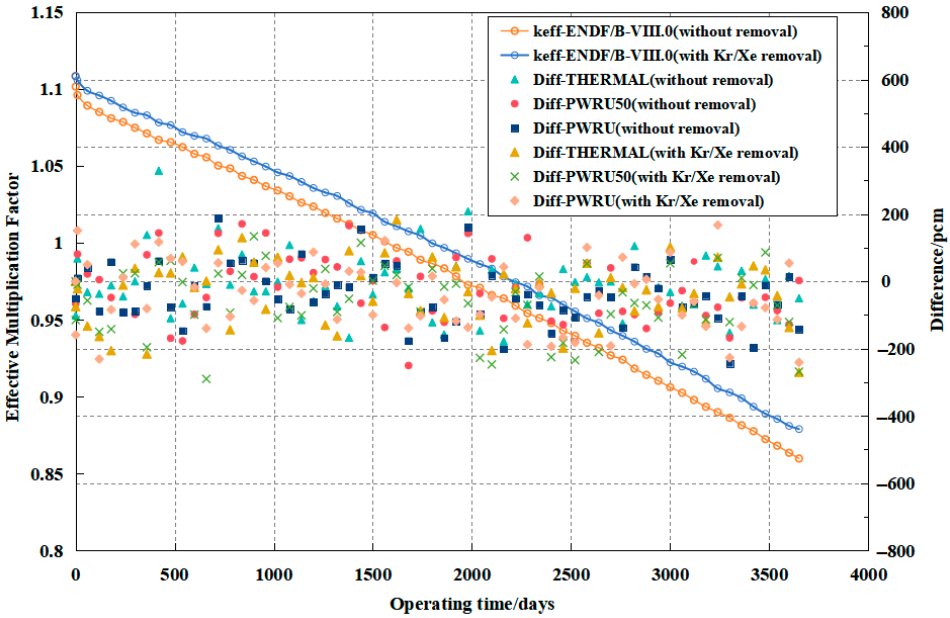


Figure 4. Comparison of core effective multiplication factors for MSRE operating with U-235.

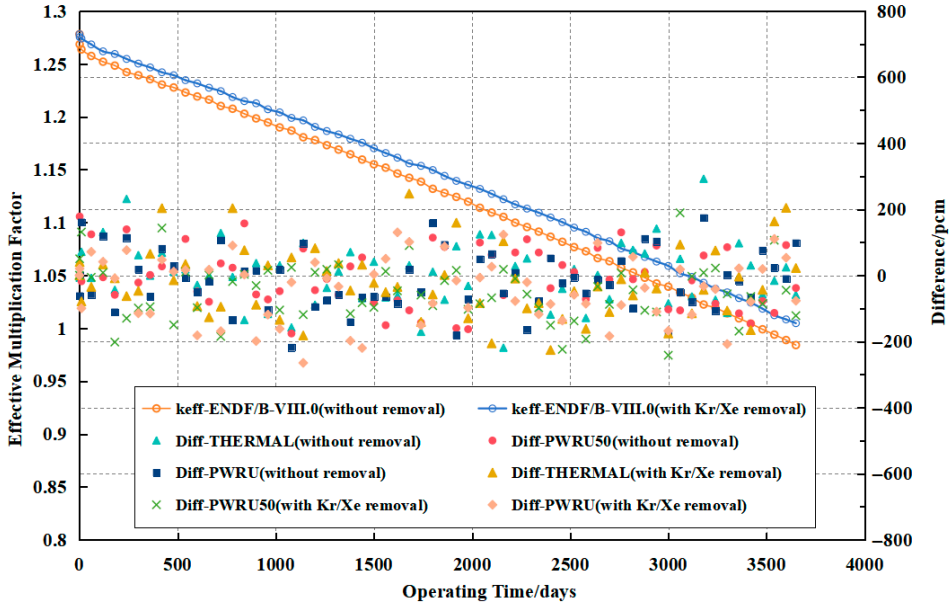


Figure 5. Comparison of core effective multiplication factors for MSRE operating with U-233.

3.2. Fission Product Source Term

Liquid-fueled molten salt reactors exhibit a fundamental characteristic where fission products generated within the molten fuel salt become distributed throughout the primary circulation loop. During operation, volatile fission gases such as krypton and xenon isotopes (Kr/Xe) are continuously purged from the system, while refractory metallic nuclides tend to accumulate locally. This operational dynamic necessitates a precise quantification of the in-core inventories for source term nuclides with distinct physicochemical properties, forming a critical basis for MSR safety design. This section analyzes discrepancies in core fission product inventories calculated using different fission yield databases for both U-235 and U-233 fuel loadings, derived from 10-year burnup simulations without reprocessing. The dissolution characteristics of the fission product elements in fluoride salts are related to the chemical properties of the elements and the chemical potential of the fluoride salts. Fission product elements can be classified based on their chemical properties as follows [17–20]:

(1) noble gases (Kr, Xe); (2) noble metals (Mo, Ru, Tc, Nb, Te, Pd, Rh, Ag, As, Se); (3) transition metals (Sn, Sb, In, Cd, Ga, Zr, Zn, Y); (4) lanthanides (La, Ce, Pr, Nd, Pm, Sm, Eu, Gd, Tb, Dy, Ho, Er); (5) active metals including alkali/alkaline earth metals (Cs, Rb, Ba, Sr); and (6) halogens (I, Br). This section compares dozens of key radioactive source term nuclides. For U-235 loading, the PWRU library (due to its best overall keff performance) was chosen for comparison against ENDF/B-VIII.0, with the results in Table 3. For U-233 loading, the PWRU50 library was similarly compared to ENDF/B-VIII.0, as shown in Table 4.

In the U-235-fueled core, after 60 days, 600 days, and 10 years of full-power operation, the relative deviations of the total activity of Kr-85, calculated using the PWRU library from the ENDF/B-VIII.0 result, was over 25%, as shown in Table 3. In ENDF/B-VIII.0, the independent fission yield of Kr-85 from U-235 at 0.0253 eV is 2.553×10^{-4}, while in the PWRU library, it is 2.280×10^{-5}. The fission yield of Kr-85 in PWRU is 91% lower than in ENDF/B-VIII.0. The actual calculated activity deviations of Kr-85 at the three time points were −27%, −26.7%, and −25.5%. To reconcile the discrepancy between the activity and fission yield deviations, the production pathways of Kr-85 were traced in Figure 6. Kr-85 production is complex, but primarily stems from Br-85 decay. With a half-life of 174 s, Br-85 has a 0.96 branching ratio to Kr-85m and a 0.04 branching ratio to Kr-85. Kr-85m has a short half-life of 4.48 h. Within the temporal resolution of depletion calculations, Br-85 decay may be approximated as an instantaneous and complete transition to Kr-85. Thus, the cumulative fission contribution to Kr-85 production can be approximately expressed as follows:

$$Y^c_{Kr85} \approx Y^d_{Kr85} + Y^c_{Br85} + Y^d_{Kr85m} \tag{1}$$

The superscript "d" denotes direct fission yield, while "c" indicates cumulative yield. By tracing the decay chain of Br-85 back three generations, six short-lived precursor nuclides were identified: Ge-85, Ge-86, Ge-87, As-85, As-86, and Se-85, as depicted in Figure 7. These nuclides can be considered to instantaneously decay into Br-85 upon formation. Summing the contributions of these precursors to Br-85 yields the cumulative fission yield of Br-85:

$$\begin{aligned} Y^c_{Br85} &= Y^c_{Ge85} \cdot y_{Se85\to Br85} + Y^d_{Br85} \\ &= \left(Y^c_{As85} \cdot y_{As85\to Se85} + Y^c_{As86} \cdot y_{As86\to Se85}\right) \cdot y_{Se85\to Br85} + Y^d_{Br85} \\ &= \left(\begin{array}{l} \left(Y^d_{Ge85} \cdot y_{Ge85\to As85} + Y^d_{As85}\right) \cdot y_{As85\to Se85} \\ +\left(Y^d_{Ge86} \cdot y_{Ge86\to As86} + Y^d_{Ge87} \cdot y_{Ge87\to As86} + Y^d_{As86}\right) \cdot y_{As86\to Se85} \end{array} \right) \cdot y_{Se85\to Br85} + Y^d_{Br85} \end{aligned} \tag{2}$$

In the equation, y denotes the decay branching ratio. By integrating the independent fission yield data from Table 5 and the decay branching ratios from Figure 7, the cumulative yield of Br-85 based on ENDF/B-VIII.0 is approximately 9.487×10^{-3}, and is 7.505×10^{-3} based on the PWRU library.

After disregarding minor reactions and the fission contributions of other actinides, the neutron flux is calculated based on the energy released by U-235 fission. Using the production and depletion terms of Kr-85, an evolution equation is formulated, leading to Equation (3).

$$\begin{aligned} &\frac{dN_{Kr85}(t)}{dt} \approx N_{U235}\sigma_f\phi \cdot Y^c_{Kr85} - N_{Kr85}(t) \cdot (\lambda_{Kr85} + \sigma_{a,Kr85}\phi) \\ &\phi \approx \frac{P}{N_{U235} \cdot V \cdot \sigma_f \cdot E_{U235}} \end{aligned} \tag{3}$$

Furthermore, assuming the U-235 concentration and all neutron reaction cross-sections remain unchanged, Equation (3) can be expressed as Equation (4).

$$\frac{dN_{Kr85}(t)}{dt} \approx C_{generate} - \lambda_{eliminate} N_{Kr85}(t) \tag{4}$$

In Equation (3), $C_{generate}$ represents the production term $N_{U235}\sigma_f\phi \cdot Y^c_{Kr85}$, and $\lambda_{eliminate}$ denotes the total disappearance rate $\lambda_{Kr85} + \sigma_{a,Kr85}\phi$ of Kr-85. Given that Kr-85 is initially absent, the analytical solution of Equation (4) can be derived as follows:

$$N_{Kr85}(t) \approx \frac{C_{generate}}{\lambda_{eliminate}}\left(1 - e^{-t\cdot\lambda_{eliminate}}\right) \quad (5)$$

From Equation (5), when the reaction cross-section, neutron flux, and U-235 concentration are assumed to be constant, the concentration of Kr-85 is approximately determined by the production term $C_{generate}$, specifically the cumulative fission yield Y^c_{Kr85} of Kr-85. Using Equation (1), the cumulative fission yield of Kr-85 based on the ENDF/B-VIII.0 library is estimated to be 9.801×10^{-3}, and is 7.665×10^{-3} based on the PWRU library. The former is approximately 22% lower than the latter, aligning with the Kr-85 activity deviation in Table 3.

Kr-85m is a significant product in the gaseous source term of molten salt reactors. When calculated using the PWRU library, its activity is lower than that from ENDF/B-VIII.0 by 19.9%, 19.4%, and 17.8% at 60 days, 600 days, and 10 years, respectively. Kr-88 shows relative deviations of over 4% at three time points. Xenon isotopes demonstrate minimal yield discrepancies, explaining the comparable keff predictions between databases—a critical observation given Xe's substantial thermal neutron capture cross-section ($\sigma_{Xe135} \approx 10^6$ barns) that would otherwise induce significant reactivity differences with even minor yield variations. Among halogen nuclides, I-133m has the largest deviation, with relative deviations of 53.2% and 32.9% at 60 and 600 days, decreasing to 2.0% at 10 years. I-133m mainly arises from direct U-235 fission, and its yield in PWRU is 56.3% lower than in ENDF/B-VIII.0.

Significant discrepancies emerge in the activity calculations of Cs-136 among active metals, with relative differences reaching 115.3%, 33.7%, and 10.1% at 60 days, 600 days, and 10 years, respectively. The PWRU library exhibits a 162% higher independent fission yield for Cs-136 compared to the reference database. Other active metals demonstrate smaller deviations. Transition metals reveal substantial activity variations across multiple nuclides: Sn-123, Sn-125, Sn-127, Sb-124, and Cd-115m show discrepancies at the tens-of-percent level, while Sb-125 displays ~10% deviation. Among noble metals, Te-129m exhibits order-of-magnitude differences in activity, with notable variations also observed in its isomers Te-125m, Te-129, and Te-131m. Lanthanide nuclides maintain minimal deviations overall. The comparative independent fission yield data for high-discrepancy radionuclides are systematically presented in Table 5.

Table 4 compares radioactive source terms for the U-233-fueled configuration, contrasting the results from the PWRU50 library with ENDF/B-VIII.0 benchmarks. The nuclides exhibiting significant discrepancies largely align with those observed in U-235-fueled cases, though with distinct magnitude variations. For the U-233 operation, the noble gases Kr-85 and Kr-85m persist as high-discrepancy species, demonstrating consistent relative deviations of ~24% and ~11% across all three temporal checkpoints (60 days, 600 days, and 10 years), respectively. Notably, the PWRU50 library predicts a 31.9%, 28.5%, and 17.5% overestimation for I-133m activity compared to ENDF/B-VIII.0 at these intervals. Cs-136 shows progressive deviation reduction from 71.4% (60d) to 26.6% (10a). When employing the PWRU50 fission yield library, the activity of Sn-123 in U-233-fueled cases exceeds reference values from the ENDF/B-VIII.0 fission yield library by 6.1%, 6.8%, and 11.4%, respectively. However, the independent fission yield for U-233→Sn-123 reported in the PWRU50 library is one order of magnitude lower than the corresponding value in ENDF/B-VIII.0. This indicates that precursor decay constitutes the dominant production pathway for Sn-123, where discrepancies in fission yields of precursor nuclides govern the observed

activity calculation deviations. Many nuclides' radioactivity deviations are due to differences in precursor nuclides, which are not individually analyzed here. Transition metals exhibit pronounced database divergences: Sn-127, Sb-124, Sb-125, Sb-127, and Cd-115m display >10% activity discrepancies. Additional high-variance nuclides include Te-125m, Te-127, Te-129m, Te-133, and Ru-106, all exceeding a 10% deviation. The primary source of Te-129m is the direct fission of actinides, and differences in its independent fission yield data explain the extreme discrepancies of activities in Table 3. In the ENDF/B-VIII.0 library, the independent yield of Te-129m from U-235 thermal fission is 1.4×10^{-7}, whereas the PWRU library reports a value three orders of magnitude higher (1.2×10^{-4}), as shown in Table 5. These systematic variations underscore the critical influence of fission yield database selection on MSR source term predictions across fuel cycles.

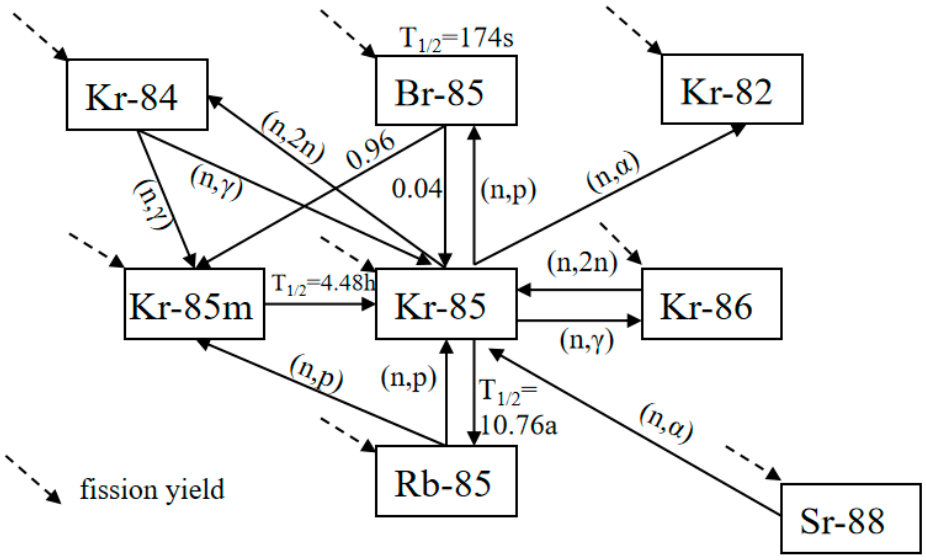


Figure 6. Reaction chain for Kr-85 production and depletion.

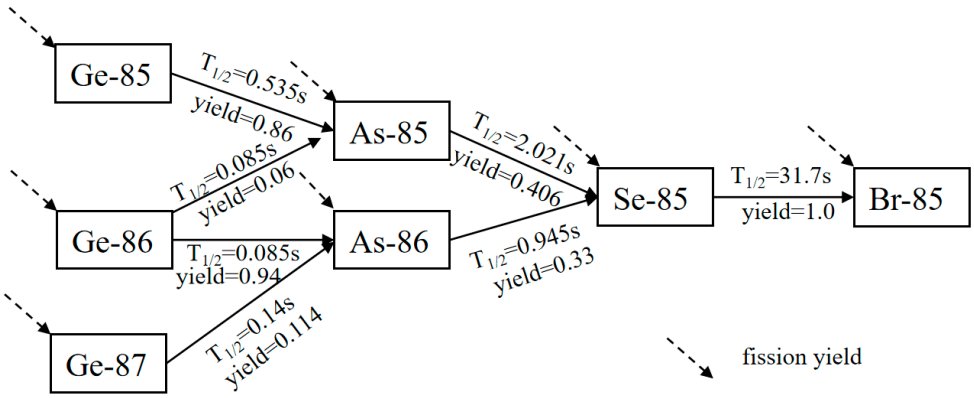


Figure 7. Production chain of Br-85.

Table 3. Radioactive nuclide activities (Bq) at different operation times for U-235 loading.

Nuclide Type	Nuclide Name	Half-Life (s)	60 Days			600 Days			10 Years		
			ENDF/B-VIII.0	PWRU	Relative Deviation	ENDF/B-VIII.0	PWRU	Relative Deviation	ENDF/B-VIII.0	PWRU	Relative Deviation
Noble Gas	Kr-83m	6.59×10^{3}	1.38×10^{15}	1.36×10^{15}	−1.1%	1.35×10^{15}	1.33×10^{15}	−1.0%	1.23×10^{15}	1.22×10^{15}	−0.7%
	Kr-85	3.39×10^{8}	7.01×10^{12}	5.11×10^{12}	−27.0%	6.60×10^{13}	4.84×10^{13}	−26.7%	2.91×10^{14}	2.17×10^{14}	−25.5%
	Kr-85m	1.61×10^{4}	2.35×10^{15}	1.88×10^{15}	−19.9%	2.28×10^{15}	1.84×10^{15}	−19.4%	2.02×10^{15}	1.66×10^{15}	−17.8%
	Kr-87	4.58×10^{3}	6.66×10^{15}	6.73×10^{15}	1.0%	6.47×10^{15}	6.53×10^{15}	0.9%	5.73×10^{15}	5.76×10^{15}	0.6%
	Kr-88	1.02×10^{4}	9.03×10^{15}	9.46×10^{15}	4.8%	8.76×10^{15}	9.18×10^{15}	4.8%	7.73×10^{15}	8.09×10^{15}	4.7%
	Xe-131m	1.02×10^{6}	8.06×10^{13}	8.05×10^{13}	−0.1%	8.87×10^{13}	8.85×10^{13}	−0.3%	9.20×10^{13}	9.15×10^{13}	−0.5%
	Xe-133	4.53×10^{5}	1.72×10^{16}	1.74×10^{16}	0.7%	1.72×10^{16}	1.73×10^{16}	0.6%	1.72×10^{16}	1.73×10^{16}	0.3%
	Xe-133m	1.89×10^{5}	1.84×10^{14}	1.88×10^{14}	1.8%	1.88×10^{14}	1.91×10^{14}	1.7%	1.98×10^{14}	2.01×10^{14}	1.4%
	Xe-135	3.29×10^{4}	1.29×10^{16}	1.29×10^{16}	0.1%	1.28×10^{16}	1.28×10^{16}	0.0%	1.14×10^{16}	1.13×10^{16}	−0.4%
	Xe-135m	9.17×10^{2}	2.06×10^{15}	2.04×10^{15}	−1.1%	2.11×10^{15}	2.08×10^{15}	−1.6%	2.29×10^{15}	2.22×10^{15}	−3.2%
Halogen	I-131	6.93×10^{5}	7.41×10^{15}	7.40×10^{15}	−0.1%	7.53×10^{15}	7.51×10^{15}	−0.3%	7.80×10^{15}	7.76×10^{15}	−0.5%
	I-133	7.49×10^{4}	1.72×10^{16}	1.73×10^{16}	0.7%	1.72×10^{16}	1.73×10^{16}	0.6%	1.71×10^{16}	1.72×10^{16}	0.3%
	I-133m	9.00×10^{0}	2.18×10^{14}	3.34×10^{14}	53.2%	2.67×10^{14}	3.55×10^{14}	32.9%	4.08×10^{14}	4.16×10^{14}	2.0%
Active Metal	Cs-136	1.14×10^{6}	1.01×10^{13}	2.17×10^{13}	115.3%	5.40×10^{13}	7.22×10^{13}	33.7%	3.66×10^{14}	4.03×10^{14}	10.1%
	Cs-137	9.49×10^{8}	6.02×10^{13}	5.95×10^{13}	−1.1%	5.92×10^{14}	5.86×10^{14}	−1.1%	3.29×10^{15}	3.25×10^{15}	−1.2%
	Cs-138	2.00×10^{3}	1.73×10^{16}	1.72×10^{16}	−0.4%	1.71×10^{16}	1.70×10^{16}	−0.5%	1.67×10^{16}	1.65×10^{16}	−1.2%
	Rb-88	1.07×10^{3}	9.08×10^{15}	9.54×10^{15}	5.1%	8.82×10^{15}	9.26×10^{15}	5.0%	7.81×10^{15}	8.18×10^{15}	4.8%
	Sr-89	4.37×10^{6}	6.83×10^{15}	7.01×10^{15}	2.6%	1.18×10^{16}	1.21×10^{16}	2.5%	1.05×10^{16}	1.07×10^{16}	2.2%
	Sr-90	9.09×10^{8}	5.87×10^{13}	5.70×10^{13}	−3.0%	5.68×10^{14}	5.51×10^{14}	−2.9%	2.93×10^{15}	2.84×10^{15}	−2.9%
	Ba-140	1.10×10^{6}	1.54×10^{16}	1.55×10^{16}	0.8%	1.59×10^{16}	1.60×10^{16}	0.9%	1.54×10^{16}	1.56×10^{16}	1.1%

Table 3. *Cont.*

Nuclide Type	Nuclide Name	Half-Life (s)	60 Days			600 Days			10 Years		
			ENDF/B-VIII.0	PWRU	Relative Deviation	ENDF/B-VIII.0	PWRU	Relative Deviation	ENDF/B-VIII.0	PWRU	Relative Deviation
Transition Metal	Sn-123	1.12×10^{7}	5.08×10^{12}	9.63×10^{12}	89.5%	1.86×10^{13}	3.46×10^{13}	85.4%	2.36×10^{13}	4.07×10^{13}	72.1%
	Sn-125	8.33×10^{5}	4.22×10^{13}	6.05×10^{13}	43.2%	4.91×10^{13}	6.73×10^{13}	37.0%	6.93×10^{13}	8.53×10^{13}	23.1%
	Sn-127	7.56×10^{3}	3.68×10^{14}	2.63×10^{14}	−28.5%	3.89×10^{14}	2.81×10^{14}	−27.7%	4.55×10^{14}	3.46×10^{14}	−24.1%
	Sb-124	5.20×10^{6}	1.48×10^{10}	2.01×10^{10}	36.5%	1.99×10^{11}	2.81×10^{11}	41.3%	2.06×10^{12}	2.87×10^{12}	39.3%
	Sb-125	8.71×10^{7}	3.17×10^{12}	3.64×10^{12}	14.7%	3.10×10^{13}	3.65×10^{13}	17.8%	1.05×10^{14}	1.24×10^{14}	18.4%
	Sb-127	3.33×10^{5}	4.08×10^{14}	4.14×10^{14}	1.4%	4.44×10^{14}	4.49×10^{14}	1.0%	5.58×10^{14}	5.61×10^{14}	0.6%
	Cd-115m	3.85×10^{6}	1.05×10^{12}	1.46×10^{12}	38.0%	1.92×10^{12}	2.55×10^{12}	33.0%	2.66×10^{12}	3.33×10^{12}	25.3%
	Zr-95	5.53×10^{6}	8.12×10^{15}	8.00×10^{15}	−1.5%	1.68×10^{16}	1.66×10^{16}	−1.4%	1.60×10^{16}	1.58×10^{16}	−1.1%
	Zr-97	6.03×10^{4}	1.55×10^{16}	1.53×10^{16}	−1.5%	1.54×10^{16}	1.52×10^{16}	−1.4%	1.49×10^{16}	1.48×10^{16}	−1.1%
	Y-90	2.30×10^{5}	5.56×10^{13}	5.46×10^{13}	−1.8%	5.66×10^{14}	5.50×10^{14}	−2.8%	2.94×10^{15}	2.85×10^{15}	−2.8%
	Y-91	5.06×10^{6}	7.56×10^{15}	7.54×10^{15}	−0.3%	1.46×10^{16}	1.45×10^{16}	−0.3%	1.31×10^{16}	1.30×10^{16}	−0.4%
Noble Metal	Te-125m	4.96×10^{6}	2.01×10^{11}	2.27×10^{11}	12.9%	6.29×10^{12}	7.40×10^{12}	17.7%	2.40×10^{13}	2.84×10^{13}	18.4%
	Te-127	3.37×10^{4}	3.94×10^{14}	3.99×10^{14}	1.4%	4.41×10^{14}	4.45×10^{14}	1.1%	5.53×10^{14}	5.57×10^{14}	0.7%
	Te-129	4.18×10^{3}	1.42×10^{15}	1.83×10^{15}	29.3%	1.50×10^{15}	1.91×10^{15}	27.6%	1.77×10^{15}	2.15×10^{15}	21.4%
	Te-129m	2.90×10^{6}	2.84×10^{10}	2.20×10^{13}	77,591.8%	9.41×10^{10}	3.28×10^{13}	34,759.3%	3.06×10^{11}	3.75×10^{13}	12,161.4%
	Te-131	1.50×10^{3}	6.96×10^{15}	7.04×10^{15}	1.1%	6.99×10^{15}	7.09×10^{15}	1.5%	7.10×10^{15}	7.27×10^{15}	2.4%
	Te-131m	1.08×10^{5}	6.08×10^{14}	4.92×10^{14}	−19.0%	6.73×10^{14}	5.18×10^{14}	−23.0%	8.59×10^{14}	5.94×10^{14}	−30.9%
	Te-132	2.77×10^{5}	1.11×10^{16}	1.10×10^{16}	−0.3%	1.11×10^{16}	1.11×10^{16}	−0.3%	1.13×10^{16}	1.13×10^{16}	−0.2%
	Te-133	7.50×10^{2}	1.05×10^{16}	1.05×10^{16}	0.2%	1.04×10^{16}	1.04×10^{16}	0.5%	1.01×10^{16}	1.03×10^{16}	1.9%
	Nb-95	3.02×10^{6}	3.66×10^{15}	3.60×10^{15}	−1.5%	1.68×10^{16}	1.65×10^{16}	−1.4%	1.60×10^{16}	1.58×10^{16}	−1.1%
	Nb-95m	3.12×10^{5}	8.21×10^{13}	8.11×10^{13}	−1.2%	1.81×10^{14}	1.79×10^{14}	−1.3%	1.73×10^{14}	1.72×10^{14}	−0.8%
	Mo-99	2.37×10^{5}	1.57×10^{16}	1.55×10^{16}	−1.2%	1.57×10^{16}	1.55×10^{16}	−1.2%	1.56×10^{16}	1.54×10^{16}	−1.2%
	Tc-99m	2.17×10^{4}	1.38×10^{16}	1.36×10^{16}	−1.2%	1.38×10^{16}	1.36×10^{16}	−1.2%	1.37×10^{16}	1.35×10^{16}	−1.2%
	Ru-106	3.23×10^{7}	1.12×10^{14}	1.16×10^{14}	3.3%	8.90×10^{14}	9.11×10^{14}	2.4%	2.97×10^{15}	2.99×10^{15}	0.5%

Table 3. *Cont.*

Nuclide Type	Nuclide Name	Half-Life (s)	60 Days			600 Days			10 Years		
			ENDF/B-VIII.0	PWRU	Relative Deviation	ENDF/B-VIII.0	PWRU	Relative Deviation	ENDF/B-VIII.0	PWRU	Relative Deviation
Lanthanides	La-140	1.45×10^{5}	1.53×10^{16}	1.54×10^{16}	0.8%	1.59×10^{16}	1.60×10^{16}	0.9%	1.57×10^{16}	1.59×10^{16}	1.1%
	Ce-141	2.81×10^{6}	1.08×10^{16}	1.09×10^{16}	0.8%	1.49×10^{16}	1.51×10^{16}	0.9%	1.46×10^{16}	1.47×10^{16}	1.0%
	Ce-144	2.46×10^{7}	1.92×10^{15}	1.89×10^{15}	−1.5%	1.08×10^{16}	1.06×10^{16}	−1.4%	1.32×10^{16}	1.31×10^{16}	−1.2%
	Pr-143	1.17×10^{6}	1.45×10^{16}	1.44×10^{16}	−0.2%	1.50×10^{16}	1.50×10^{16}	−0.1%	1.43×10^{16}	1.43×10^{16}	0.1%
	Pr-144	1.04×10^{3}	1.93×10^{15}	1.91×10^{15}	−1.5%	1.08×10^{16}	1.06×10^{16}	−1.4%	1.32×10^{16}	1.31×10^{16}	−1.2%
	Nd-147	9.49×10^{5}	5.64×10^{15}	5.73×10^{15}	1.6%	5.73×10^{15}	5.82×10^{15}	1.6%	5.63×10^{15}	5.72×10^{15}	1.7%
	Pm-147	8.28×10^{7}	1.82×10^{14}	1.85×10^{14}	1.6%	1.87×10^{15}	1.90×10^{15}	1.6%	4.03×10^{15}	4.10×10^{15}	1.7%
	Pm-148	4.64×10^{5}	3.49×10^{13}	3.54×10^{13}	1.5%	4.43×10^{14}	4.49×10^{14}	1.5%	1.27×10^{15}	1.29×10^{15}	1.7%

Table 4. Radioactive nuclide activities (Bq) at different operation times for U-233 loading.

Nuclide Type	Nuclide Name	Half-Life (s)	60 Days			600 Days			10 Years		
			ENDF/B-VIII.0	PWRU	Relative Deviation	ENDF/B-VIII.0	PWRU	Relative Deviation	ENDF/B-VIII.0	PWRU	Relative Deviation
Noble Gas	Kr-83m	6.59×10^{3}	2.60×10^{15}	2.61×10^{15}	0.5%	2.53×10^{15}	2.55×10^{15}	0.5%	2.25×10^{15}	2.26×10^{15}	0.6%
	Kr-85	3.39×10^{8}	1.30×10^{13}	9.80×10^{12}	−24.8%	1.23×10^{14}	9.25×10^{13}	−24.6%	5.39×10^{14}	4.09×10^{14}	−24.1%
	Kr-85m	1.61×10^{4}	3.87×10^{15}	3.43×10^{15}	−11.4%	3.77×10^{15}	3.34×10^{15}	−11.3%	3.32×10^{15}	2.96×10^{15}	−10.8%
	Kr-87	4.58×10^{3}	1.02×10^{16}	1.05×10^{16}	2.6%	9.97×10^{15}	1.02×10^{16}	2.6%	8.81×10^{15}	9.01×10^{15}	2.3%
	Kr-88	1.02×10^{4}	1.33×10^{16}	1.36×10^{16}	2.7%	1.29×10^{16}	1.33×10^{16}	2.7%	1.14×10^{16}	1.17×10^{16}	2.8%
	Xe-131m	1.02×10^{6}	1.01×10^{14}	1.00×10^{14}	−1.3%	1.11×10^{14}	1.09×10^{14}	−1.3%	1.10×10^{14}	1.09×10^{14}	−1.4%
	Xe-133	4.53×10^{5}	1.55×10^{16}	1.57×10^{16}	1.0%	1.55×10^{16}	1.57×10^{16}	0.9%	1.58×10^{16}	1.59×10^{16}	0.6%
	Xe-133m	1.89×10^{5}	2.67×10^{14}	2.68×10^{14}	0.2%	2.67×10^{14}	2.67×10^{14}	0.2%	2.64×10^{14}	2.65×10^{14}	0.2%
	Xe-135	3.29×10^{4}	1.31×10^{16}	1.29×10^{16}	−1.1%	1.30×10^{16}	1.28×10^{16}	−1.2%	1.17×10^{16}	1.16×10^{16}	−1.3%
	Xe-135m	9.17×10^{2}	3.39×10^{15}	3.32×10^{15}	−2.1%	3.39×10^{15}	3.31×10^{15}	−2.3%	3.34×10^{15}	3.24×10^{15}	−3.1%

Table 4. *Cont.*

Nuclide Type	Nuclide Name	Half-Life (s)	60 Days			600 Days			10 Years		
			ENDF/B-VIII.0	PWRU	Relative Deviation	ENDF/B-VIII.0	PWRU	Relative Deviation	ENDF/B-VIII.0	PWRU	Relative Deviation
Halogen	I-131	6.93×10^{5}	9.34×10^{15}	9.21×10^{15}	−1.3%	9.38×10^{15}	9.25×10^{15}	−1.4%	9.34×10^{15}	9.21×10^{15}	−1.4%
	I-133	7.49×10^{4}	1.54×10^{16}	1.55×10^{16}	1.0%	1.54×10^{16}	1.55×10^{16}	0.9%	1.56×10^{16}	1.57×10^{16}	0.6%
	I-133m	9.00×10^{0}	9.28×10^{14}	1.22×10^{15}	31.9%	9.41×10^{14}	1.21×10^{15}	28.5%	9.62×10^{14}	1.13×10^{15}	17.5%
Active Metal	Cs-136	1.14×10^{6}	1.64×10^{14}	2.82×10^{14}	71.4%	2.04×10^{14}	3.27×10^{14}	60.4%	4.55×10^{14}	5.77×10^{14}	26.6%
	Cs-137	9.49×10^{8}	6.66×10^{13}	6.54×10^{13}	−1.8%	6.54×10^{14}	6.42×10^{14}	−1.8%	3.60×10^{15}	3.53×10^{15}	−1.8%
	Cs-138	2.00×10^{3}	1.49×10^{16}	1.46×10^{16}	−2.3%	1.49×10^{16}	1.46×10^{16}	−2.4%	1.49×10^{16}	1.45×10^{16}	−2.7%
	Rb-88	1.07×10^{3}	1.42×10^{16}	1.41×10^{16}	−0.4%	1.38×10^{16}	1.37×10^{16}	−0.4%	1.22×10^{16}	1.22×10^{16}	−0.2%
	Sr-89	4.37×10^{6}	9.26×10^{15}	9.08×10^{15}	−2.0%	1.61×10^{16}	1.58×10^{16}	−2.0%	1.43×10^{16}	1.40×10^{16}	−1.9%
	Sr-90	9.09×10^{8}	6.98×10^{13}	6.78×10^{13}	−2.8%	6.77×10^{14}	6.58×10^{14}	−2.8%	3.52×10^{15}	3.42×10^{15}	−2.7%
	Ba-140	1.10×10^{6}	1.60×10^{16}	1.59×10^{16}	−0.6%	1.65×10^{16}	1.64×10^{16}	−0.6%	1.61×10^{16}	1.60×10^{16}	−0.2%
Transition Metal	Sn-123	1.12×10^{7}	1.67×10^{13}	1.77×10^{13}	6.1%	5.78×10^{13}	6.18×10^{13}	6.8%	5.76×10^{13}	6.41×10^{13}	11.4%
	Sn-125	8.33×10^{5}	2.05×10^{14}	1.94×10^{14}	−5.7%	2.07×10^{14}	1.96×10^{14}	−5.3%	2.00×10^{14}	1.92×10^{14}	−4.0%
	Sn-127	7.56×10^{3}	1.03×10^{15}	8.96×10^{14}	−13.0%	1.02×10^{15}	8.88×10^{14}	−13.2%	9.83×10^{14}	8.49×10^{14}	−13.6%
	Sb-124	5.20×10^{6}	4.55×10^{10}	1.90×10^{11}	316.7%	6.52×10^{11}	7.72×10^{11}	18.4%	5.78×10^{12}	4.71×10^{12}	−18.5%
	Sb-125	8.71×10^{7}	1.04×10^{13}	1.28×10^{13}	22.8%	1.02×10^{14}	1.21×10^{14}	18.8%	2.74×10^{14}	3.25×10^{14}	18.6%
	Sb-127	3.33×10^{5}	1.44×10^{15}	1.92×10^{15}	32.6%	1.44×10^{15}	1.89×10^{15}	31.6%	1.38×10^{15}	1.76×10^{15}	27.7%
	Cd-115m	3.85×10^{6}	1.35×10^{12}	1.64×10^{12}	21.2%	2.34×10^{12}	2.80×10^{12}	19.6%	2.90×10^{12}	3.42×10^{12}	17.7%
	Zr-95	5.53×10^{6}	8.02×10^{15}	7.90×10^{15}	−1.5%	1.66×10^{16}	1.64×10^{16}	−1.5%	1.60×10^{16}	1.58×10^{16}	−1.2%
	Zr-97	6.03×10^{4}	1.42×10^{16}	1.39×10^{16}	−2.1%	1.41×10^{16}	1.38×10^{16}	−2.0%	1.40×10^{16}	1.38×10^{16}	−1.6%
	Y-90	2.30×10^{5}	6.63×10^{13}	6.51×10^{13}	−1.8%	6.76×10^{14}	6.57×10^{14}	−2.7%	3.53×10^{15}	3.43×10^{15}	−2.7%
	Y-91	5.06×10^{6}	8.53×10^{15}	8.51×10^{15}	−0.2%	1.65×10^{16}	1.65×10^{16}	−0.2%	1.50×10^{16}	1.49×10^{16}	−0.3%

Table 4. *Cont.*

Nuclide Type	Nuclide Name	Half-Life (s)	60 Days			600 Days			10 Years		
			ENDF/B-VIII.0	PWRU	Relative Deviation	ENDF/B-VIII.0	PWRU	Relative Deviation	ENDF/B-VIII.0	PWRU	Relative Deviation
Noble Metal	Te-125m	4.96×10^{6}	6.40×10^{11}	8.10×10^{11}	26.7%	2.07×10^{13}	2.46×10^{13}	18.9%	6.32×10^{13}	7.50×10^{13}	18.7%
	Te-127	3.37×10^{4}	1.39×10^{15}	1.85×10^{15}	33.1%	1.43×10^{15}	1.89×10^{15}	32.4%	1.37×10^{15}	1.76×10^{15}	28.4%
	Te-129	4.18×10^{3}	4.11×10^{15}	4.23×10^{15}	3.0%	4.09×10^{15}	4.26×10^{15}	4.2%	3.92×10^{15}	4.11×10^{15}	4.7%
	Te-129m	2.90×10^{6}	4.17×10^{13}	2.29×10^{14}	448.7%	5.69×10^{13}	3.14×10^{14}	452.4%	4.83×10^{13}	2.75×10^{14}	469.3%
	Te-131	1.50×10^{3}	7.03×10^{15}	7.06×10^{15}	0.4%	7.04×10^{15}	7.09×10^{15}	0.7%	7.13×10^{15}	7.26×10^{15}	1.7%
	Te-131m	1.08×10^{5}	2.90×10^{15}	2.67×10^{15}	−7.9%	2.87×10^{15}	2.62×10^{15}	−8.9%	2.70×10^{15}	2.36×10^{15}	−12.6%
	Te-132	2.77×10^{5}	1.24×10^{16}	1.17×10^{16}	−5.6%	1.24×10^{16}	1.17×10^{16}	−5.5%	1.24×10^{16}	1.18×10^{16}	−4.6%
	Te-133	7.50×10^{2}	6.91×10^{15}	5.53×10^{15}	−20.0%	6.96×10^{15}	5.65×10^{15}	−18.8%	7.27×10^{15}	6.29×10^{15}	−13.5%
	Nb-95	3.02×10^{6}	3.61×10^{15}	3.56×10^{15}	−1.5%	1.66×10^{16}	1.64×10^{16}	−1.5%	1.60×10^{16}	1.58×10^{16}	−1.1%
	Nb-95m	3.12×10^{5}	8.10×10^{13}	8.22×10^{13}	1.4%	1.80×10^{14}	1.79×10^{14}	−0.1%	1.73×10^{14}	1.73×10^{14}	0.1%
	Mo-99	2.37×10^{5}	1.28×10^{16}	1.28×10^{16}	0.5%	1.29×10^{16}	1.29×10^{16}	0.4%	1.32×10^{16}	1.32×10^{16}	0.1%
	Tc-99m	2.17×10^{4}	1.12×10^{16}	1.13×10^{16}	0.5%	1.13×10^{16}	1.13×10^{16}	0.4%	1.16×10^{16}	1.16×10^{16}	0.1%
	Ru-106	3.23×10^{7}	7.00×10^{13}	8.75×10^{13}	24.9%	5.82×10^{14}	6.90×10^{14}	18.5%	2.28×10^{15}	2.41×10^{15}	5.6%
Lanthanides	La-140	1.45×10^{5}	1.60×10^{16}	1.59×10^{16}	−0.7%	1.66×10^{16}	1.65×10^{16}	−0.6%	1.63×10^{16}	1.63×10^{16}	−0.2%
	Ce-141	2.81×10^{6}	1.22×10^{16}	1.25×10^{16}	2.4%	1.67×10^{16}	1.71×10^{16}	2.4%	1.61×10^{16}	1.65×10^{16}	2.3%
	Ce-144	2.46×10^{7}	1.67×10^{15}	1.63×10^{15}	−2.5%	9.40×10^{15}	9.18×10^{15}	−2.4%	1.19×10^{16}	1.16×10^{16}	−2.0%
	Pr-143	1.17×10^{6}	1.47×10^{16}	1.44×10^{16}	−2.2%	1.54×10^{16}	1.50×10^{16}	−2.1%	1.47×10^{16}	1.45×10^{16}	−1.6%
	Pr-144	1.04×10^{3}	1.68×10^{15}	1.65×10^{15}	−2.3%	9.42×10^{15}	9.19×10^{15}	−2.4%	1.19×10^{16}	1.16×10^{16}	−2.0%
	Nd-147	9.49×10^{5}	4.42×10^{15}	4.54×10^{15}	2.7%	4.54×10^{15}	4.66×10^{15}	2.7%	4.63×10^{15}	4.75×10^{15}	2.6%
	Pm-147	8.28×10^{7}	1.43×10^{14}	1.47×10^{14}	2.7%	1.49×10^{15}	1.53×10^{15}	2.7%	3.38×10^{15}	3.47×10^{15}	2.7%
	Pm-148	4.64×10^{5}	2.37×10^{13}	2.44×10^{13}	2.7%	3.06×10^{14}	3.14×10^{14}	2.5%	9.38×10^{14}	9.61×10^{14}	2.4%

Table 5. Independent fission yields of selected fission products in thermal fission.

Nuclide	U-235 Fission System		U-233 Fission System	
	ENDF/B-VIII.0	PWRU	ENDF/B-VIII.0	PWRU50
Br85	2.350×10^{-3}	1.690×10^{-3}	8.867×10^{-3}	5.780×10^{-3}
Kr85	2.553×10^{-4}	2.280×10^{-5}	9.558×10^{-4}	2.130×10^{-4}
Se-85	4.467×10^{-3}	4.600×10^{-3}	5.881×10^{-3}	7.100×10^{-3}
As-86	1.992×10^{-4}	1.130×10^{-3}	4.275×10^{-4}	3.800×10^{-4}
As-85	1.214×10^{-3}	2.010×10^{-3}	1.051×10^{-3}	1.390×10^{-3}
Ge-85	2.130×10^{-5}	6.440×10^{-5}	1.317×10^{-5}	1.800×10^{-5}
Ge-86	6.287×10^{-3}	1.140×10^{-5}	2.180×10^{-6}	1.440×10^{-6}
Ge-87	2.196×10^{-5}	1.830×10^{-6}	3.590×10^{-8}	7.930×10^{-8}
I-133m	8.251×10^{-4}	1.290×10^{-3}	3.561×10^{-3}	4.710×10^{-3}
Cs-136	2.769×10^{-5}	7.260×10^{-5}	6.496×10^{-4}	1.120×10^{-3}
Sn-123	8.039×10^{-6}	1.620×10^{-5}	1.151×10^{-4}	1.520×10^{-5}
Sn-125	8.542×10^{-5}	1.060×10^{-4}	5.171×10^{-4}	3.090×10^{-4}
Sn-127	8.667×10^{-4}	4.720×10^{-4}	3.395×10^{-3}	2.600×10^{-3}
Sb-124	7.609×10^{-8}	6.960×10^{-8}	1.387×10^{-7}	7.990×10^{-7}
Sb-125	2.740×10^{-7}	1.200×10^{-6}	3.220×10^{-6}	2.240×10^{-5}
Cd-115m	5.530×10^{-8}	3.640×10^{-8}	4.420×10^{-7}	4.020×10^{-7}
Te-125m	2.300×10^{-13}	1.380×10^{-9}	2.690×10^{-11}	4.870×10^{-8}
Te-129	5.730×10^{-8}	1.480×10^{-4}	9.234×10^{-5}	1.240×10^{-3}
Te-131	9.699×10^{-4}	1.190×10^{-3}	5.025×10^{-3}	4.280×10^{-3}
Te-129m	1.400×10^{-7}	1.200×10^{-4}	2.261×10^{-4}	1.240×10^{-3}
Te-131m	2.333×10^{-3}	1.900×10^{-3}	1.117×10^{-2}	1.030×10^{-2}
Te-132	1.531×10^{-2}	1.540×10^{-2}	3.580×10^{-2}	3.090×10^{-2}
Te-133	1.148×10^{-2}	1.320×10^{-2}	1.286×10^{-2}	1.150×10^{-2}
Ru-106	9.069×10^{-9}	1.200×10^{-5}	5.567×10^{-5}	4.380×10^{-5}

3.3. Shutdown Decay Heat

While the effective multiplication factor provides a global assessment of neutronically significant fission products with substantial absorption cross-sections, a decay heat analysis serves as a complementary metric for evaluating collective discrepancies among radioactive fission products. This section investigates the impact of ORIGEN2 fission yield libraries on post-shutdown decay heat predictions under full-power operation. The simulations evaluate equilibrium decay heat conditions attained after 600 days of continuous operation without Kr/Xe removal, comparing total decay heat and gaseous component contributions for both U-235 and U-233 fuel configurations. Gaseous decay heat calculations specifically consider all Kr/Xe isotopes present at shutdown as initial inventories for a subsequent decay analysis.

Figure 8 shows that in U-235 loading, the total shutdown decay heat from the PWRU library aligns closely with ENDF/B-VIII.0 results within one year, with deviations mostly between −1% and 1%. Initially, the gaseous decay heat deviations are near zero but rise above 20% after 60 days as Kr-85 becomes the main contributor. Figure 9 presents the decay

heat results for U-233 loading using the PWRU50 library versus ENDF/B-VIII.0, yielding similar conclusions: total decay heat deviations stay under 1% within a year, while gaseous decay heat power differences exceed 20% after 60 days. The ORIGEN2 fission yield library shows deviations in simulating the decay heat power of fission gases in molten salt reactors, and this issue is of great significance. MSRs are typically equipped with an offgas treatment system, such as a holdup coil and activated charcoal bed, which serves to temporarily retain radioactive offgas and reduce radioactive emissions. However, inaccuracies in simulating the decay heat power of the offgas may impact the design of the offgas treatment system.

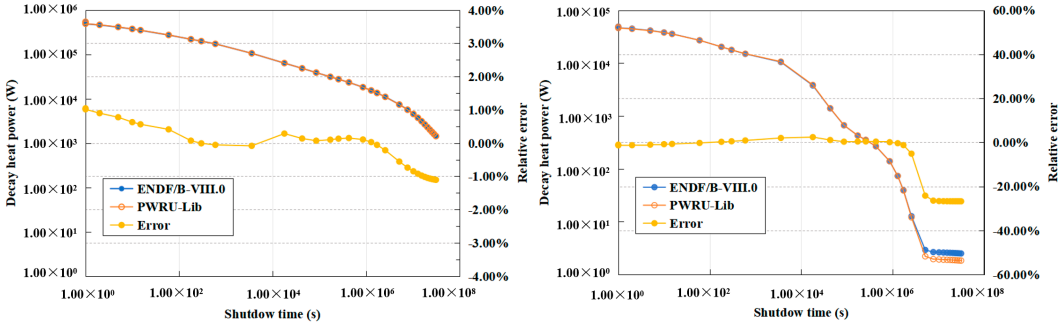


Figure 8. Comparison of decay heat power after shutdown for U-235 loading following 600 Days of full-power operation. (**a**) Total decay heat. (**b**) Gaseous decay heat.

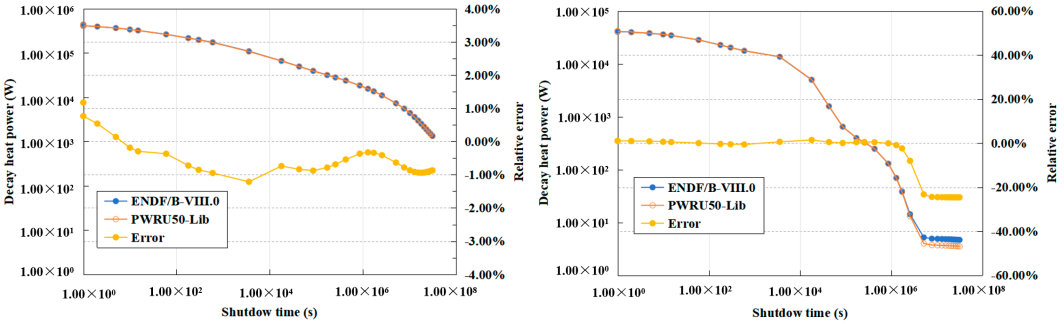


Figure 9. Comparison of decay heat power after shutdown for U-233 loading following 600 days of full-power operation. (**a**) Total decay heat. (**b**) Gaseous decay heat.

4. Conclusions

In this study, we conducted a comprehensive evaluation of ORIGEN2's fission yield libraries (THERMAL, PWRU, and PWRU50) against the modern ENDF/B-VIII.0 library for molten salt reactor (MSR) burnup calculations, using Oak Ridge National Laboratory's Molten Salt Reactor Experiment (MSRE) data as a benchmark. For the effective multiplication factor (keff), the PWRU library provided the closest alignment with ENDF/B-VIII.0 for the U-235-fueled MSRE, while the PWRU50 library showed the smallest keff deviations for the U-233-fueled configurations. Regarding fission product source terms, significant discrepancies were observed in the activity of key radionuclides in the MSR.

When the MSRE operates at full power with U-235 loading for 60 days, 600 days, and 10 years, the relative deviations in the total activity of key radionuclides calculated using the PWRU library are summarized as follows:

(1) The deviations for Kr-85 are −27.0%, −26.7%, and −25.5%, and for Kr-85m they are −19.9%, −19.4%, and −17.8%.
(2) The deviations for I-133m are 53.2%, 32.9%, and 2.0%.

(3) The deviations for Cs-136 are 115.3%, 33.7%, and 10.1%.
(4) The deviations for Sn-123 are 89.5%, 85.4%, and 72.1%; for Sn-125, they are 43.2%, 37.0%, and 23.1%; for Sn-127, they are −28.5%, −27.7%, and −24.1%; for Sb-124, they are 36.5%, 41.3%, and 39.3%; and for Cd-115m, they are 38.0%, 33.0%, and 25.3%.
(5) The deviations for Te-125m are 12.9%, 17.7%, and 18.4%; for Te-129, they are 29.3%, 27.6%, and 21.4%. Te-129m is higher by 3–4 orders of magnitude, and for Te-131m, the deviations are −19.0%, −23.0%, and −30.9%.

For the U-233-fueled MSRE configurations at 60 days, 600 days, and 10 years of full-power operation, the PWRU50 library exhibits significant isotopic activity deviations compared to the reference, as summarized below:

(1) The deviations for Kr-85 are −24.8%, −24.6%, and −24.1%, and for Kr-85m they are −11.4%, −11.3%, and −10.8%.
(2) The deviations for I-133m are 31.9%, 28.5%, and 17.5%.
(3) The deviations for Cs-136 are 71.4%, 60.4%, and 26.6%.
(4) The deviations for Sn-123 are 6.1%, 6.8%, and 11.4%; for Sn-127, they are −13.0%, −13.2%, and −13.6%; for Sb-124, they are 316.7%, 18.4%, and −18.5%; for Sb-125, they are 22.8%, 18.8%, and −18.6%; and for Cd-115m, they are 21.2%, 19.6%, and 17.7%.
(5) The deviations for Te-125m are 26.7%, 18.9%, and 18.7%; for Te-127, they are 33.1%, 32.4%, and 28.4%; for Te-129, they are 29.3%, 27.6%, and 21.4%; for Te-129m, they are 448.7%, 452.4%, and 469.3%; for Te-131m, they are −7.9%, −8.9%, and −12.6%; for Te-133, they are −20.0%, −18.8%, and −13.5%; and for Ru-106, they are 24.9%, 18.5% and 5.6%.

Furthermore, in shutdown decay heat simulations, both the U-235-fueled MSRE modeled with the PWRU library and the U-233-fueled MSRE using the PWRU50 library exhibit maximum total decay heat deviations within approximately 1% during the first post-shutdown year following 600 full-power operational days. However, the fission gas decay heat contributions demonstrate significant library-dependent discrepancies. For the PWRU-modeled U-235 case and the PWRU50-modeled U-233 case, gaseous decay heat deviations exceeded 20% beyond 60 days post-shutdown compared to the results from the ENDF/B-VIII.0 library, which was caused by the production difference of Kr-85.

This study offers a quantitative analysis of discrepancies arising from the application of ORIGEN2 fission yield libraries versus the modern ENDF/B-VIII.0 database in molten salt reactor (MSR) burnup analysis. To enhance predictive accuracy, future efforts should focus on refining the fission yield databases in MSR burnup codes based on experimental fission product data from MSRs. Such refinements will enable more accurate predictions of burnup characteristics and source term data, thereby offering stronger support for the safety design and operation of next-generation molten salt reactors.

Author Contributions: Conceptualization, Y.Z. (Yunfei Zhang), G.Z. and Y.Z. (Yang Zou); Methodology, Y.Z. (Yunfei Zhang); Software, Y.Z. (Yunfei Zhang); Resources, G.Z.; Data curation, J.G., B.Z. and A.Z.; Writing—original draft, Y.Z. (Yunfei Zhang); Writing—review & editing, G.Z., Y.Z. (Yang Zou), J.G., B.Z. and R.Y.; Project administration, Y.Z. (Yang Zou). All authors have read and agreed to the published version of the manuscript.

Funding: This study is supported by funds provided by the following sources: the Chinese Academy of Sciences Special Research Assistant Project, and the Frontier Science Key Program of Chinese Academy of Sciences (No. QYZDY-SSW-JSC016).

Data Availability Statement: Data are contained within the article.

Conflicts of Interest: The authors declare no conflict of interest.

References

1. Serp, J.; Allibert, M.; Beneš, O.; Delpech, S.; Feynberg, O.; Ghetta, V.; Heuer, D.; Holcomb, D.; Ignatiev, V.; Kloosterman, J.L.; et al. The molten salt reactor (MSR) in generation IV: Overview and perspectives. *Prog. Nucl. Energy* **2014**, *77*, 308–319. [CrossRef]
2. LeBlanc, D. Molten salt reactors: A new beginning for an old idea. *Nucl. Eng. Des.* **2010**, *240*, 1644–1656. [CrossRef]
3. Locatelli, G.; Mancini, M.; Todeschini, N. Generation IV nuclear reactors: Current status and future prospects. *Energy Policy* **2013**, *61*, 1503–1520. [CrossRef]
4. Robertson, R.C. *MSRE Design and Operation Report I: Description of Reactor Design Oak Ridge National Laboratory*; Report No. ORNL-TM-728; Oak Ridge National Lab: Oak Ridge, TN, USA, 1965.
5. Lee, K.O.; Kropaczek, D.; Graham, A.M. *Noble Gas Transport in the MSRE*; Oak Ridge National Laboratory (ORNL): Oak Ridge, TN, USA, 2023.
6. Croff, A.G. *User's Manual for the ORIGEN2 Computer Code*; Oak Ridge National Lab: Oak Ridge, TN, USA, 1980.
7. Croff, A.G. ORIGEN2: A versatile computer code for calculating the nuclide compositions and characteristics of nuclear materials. *Nucl. Technol.* **1983**, *62*, 335–352. [CrossRef]
8. Zhu, G.; Yan, R.; Dai, M.; Yu, S.; Kang, X.; Yu, X.; Cai, X.; Liu, G.; Zou, Y. Monte Carlo burnup code development based on multi-group cross section method. *Prog. Nucl. Energy* **2019**, *110*, 24–29. [CrossRef]
9. England, T.R.; Schenter, R.E. *ENDF/B-IV Fission-Product Files: Summary of Major Nuclide Data*; Los Alamos National Lab (LANL): Los Alamos, NM, USA, 1975.
10. Brown, D.A.; Chadwick, M.B.; Capote, R.; Kahler, A.C.; Trkov, A.; Herman, M.W.; Sonzogni, A.A.; Danon, Y.; Carlson, A.D.; Dunn, M.; et al. ENDF/B-VIII.0: The 8th major release of the nuclear reaction data library with CIELO-project cross sections, new standards and thermal scattering data. *Nucl. Data Sheets* **2018**, *148*, 1–142. [CrossRef]
11. Zhang, Y.; Zou, Y.; Yan, R.; Zhu, G.; Zhang, Q. A Comprehensive Depletion Code Mact For Molten Salt Reactors. Available online: https://ssrn.com/abstract=5204609 (accessed on 3 July 2025).
12. Pusa, M.; Leppänen, J. Computing the matrix exponential in burnup calculations. *Nucl. Sci. Eng.* **2010**, *164*, 140–150. [CrossRef]
13. Pusa, M. Rational approximations to the matrix exponential in burnup calculations. *Nucl. Sci. Eng.* **2011**, *169*, 155–167. [CrossRef]
14. Cetnar, J.; Stanisz, P.; Oettingen, M. Linear chain method for numerical modelling of burnup systems. *Energies* **2021**, *14*, 1520. [CrossRef]
15. Romano, P.K.; Horelik, N.E.; Herman, B.R.; Nelson, A.G.; Forget, B.; Smith, K. OpenMC: A state-of-the-art Monte Carlo code for research and development. *Ann. Nucl. Energy* **2015**, *82*, 90–97. [CrossRef]
16. Vicente Valdez, P., Jr.; Betzler, B.R.; Wieselquist, W.A.; Fratoni, M. *Modeling Molten Salt Reactor Fission Product Removal with SCALE*; Oak Ridge National Laboratory (ORNL): Oak Ridge, TN, USA, 2020.
17. Bell, M.J. *Calculated Radioactivity of MSRE Fuel Salt*; ORNL-TM-2970; Oak Ridge National Laboratory (ORNL): Oak Ridge, TN, USA, 1970.
18. Compere, E.L.; Kirslis, S.S.; Bohlmann, E.G.; Blankenship, F.F.; Grimes, W.R. *Fission Product Behavior in the Molten Salt Reactor Experiment*; ORNL-4865; Oak Ridge National Laboratory (ORNL): Oak Ridge, TN, USA, 1975.
19. Taylor, Z.; Salko, R.K.; Collins, B.S. *Implementation of General Species Transport Capability into VERA-CS for Molten Salt Reactor Analysis*; Transactions of the American Nuclear Society: Westmont, IL, USA, 2018; Volume 118, pp. 1061–1064.
20. Haubenreich, P.N. *Prediction of Effective Yields of Delayed Neutrons in MSRE*; ORNL-TM-380; Oak Ridge National Laboratory (ORNL): Oak Ridge, TN, USA, 1962.

Disclaimer/Publisher's Note: The statements, opinions and data contained in all publications are solely those of the individual author(s) and contributor(s) and not of MDPI and/or the editor(s). MDPI and/or the editor(s) disclaim responsibility for any injury to people or property resulting from any ideas, methods, instructions or products referred to in the content.